REC protein family expansion by the emergence of a new signaling pathway

Megan E. Garber[1, 2], Vered Frank[2], Alexey E. Kazakov[6], Matthew R. Incha[2,4], Alberto A. Nava[2,5], Hanqiao Zhang[2,6], Jay D. Keasling[2,4,5,7,8], Lara Rajeev[2], Aindrila Mukhopadhyay*[1,2,3]

Author Affiliations:

1. University of California, Berkeley Department of Comparative Biochemistry
2. Lawrence Berkeley National Laboratory, Biological Systems and Engineering Division
3. University of California, Berkeley Department of Bioengineering
4. University of California, Berkeley Department of Plant and Microbial Biology
5. University of California, Berkeley Department of Chemical and Biomolecular Engineering
6. Lawrence Berkeley National Laboratory, Environmental Genomics and Systems Biology Division
7. Center for Biosustainability, Danish Technical University, Lyngby, Denmark
8. Center for Synthetic Biochemistry, Shenzhen Institutes for Advanced Technologies, Shenzhen, China

* Correspondence: amukhopadhyay@lbl.gov

Abstract

This report presents multi-genomes and experimental evidence that REC protein family expansion occurs when the emergence of new pathways give rise to functional discordance. Specificity between REC-domain containing response regulators with paired histidine kinases are under negative purifying selection, constrained by the presence of other bacterial two-component systems signaling cascades that share sequence and structural identity. Presuming that the two-component systems can evolve by neutral drift when these constraints are relaxed, how might the REC protein family expand when constraints remain intact? Using an unsupervised machine learning approach to observe the sequence landscape of REC domains across long phylogenetic distances, we find that within-gene-recombination, a subcategory of gene conversion, switched the effector domain, and consequently the regulatory context of a duplicated response regulator from transcriptional regulation by σ54 to σ70. We determined that the recombined response regulator diverged from its parent by positive episodic diversifying selection, giving rise to two new residues. Functional experiments of the parent of recombined response regulators in our model system, *Pseudomonas putida* KT2440, revealed that the parent and recombined response regulators sense and respond to carboxylic acids and that the two new residues in the recombined regulator form a new interaction interface and prevent crosstalk. Overall, our study finds genetic perturbations can create conditions of functional discordance, whereby the REC protein family can evolve by positive diversifying selection.

Introduction

Large protein families are a group of proteins that share a common ancestor, showing strong sequence conservation across long phylogenetic distances (Heger and Holm 2003; Buljan and Bateman 2009; Finn et al. 2017; El-Gebali et al. 2019). Amino acid consensus motifs are used to understand protein family function and specificity; active-site residues are fixed and tell

47 us about the chemistry the protein family performs or undergoes, while variable residues
48 determine the protein's specificity for different substrates or ligands. These variable, specificity-
49 determining, residues form the molecular basis of tightly regulated signal transduction (Pao and
50 Saier 1995; Capra and Laub 2012; Hirakawa et al. 2020), such as those found in phosphorelay
51 receiver (REC) domains of response regulators, allowing for specific, context dependent, protein-
52 protein interactions.

53 Members of the REC protein family (PF00072), function as phosphorelay receivers in
54 bacterial signaling cascades called two-component systems. Most bacterial genomes encode
55 dozens to over a hundred of these systems (Galperin 2006; Galperin 2018; Gumerov et al. 2020).
56 Two component systems modulate important functions in bacterial pathogenesis, antibiotic
57 resistance, nutrient use (e.g. carbon, nitrogen, or phosphate utilization), fitness in a microbiome
58 context and a vast number of other functions that are responsive to signals (Gumerov et al. 2020;
59 Hirakawa et al. 2020), making them attractive targets for addressing infection (Hirakawa et al.
60 2020), pathogenesis (Tiwari et al. 2017; Wang et al. 2021) and for beneficial applications in synbio
61 and biotechnology (McClune et al. 2019; Schmidl et al. 2019; Volke et al. 2020). In the case of
62 signaling systems and the REC protein family, despite large numbers of highly analogous systems
63 encoded in a single genome, in these signaling cascades, membrane bound histidine kinases
64 sense a signal, autophosphorylate, and with precise biochemical specificity, phosphorylate its
65 cognate response regulator (Stock et al. 2000; Laub and Goulian 2007; Papon and Stock 2019).
66 The phosphorylated cognate response regulator then regulates cellular functions, mainly via
67 transcription, chemotaxis, or modulation of second messengers (Figure 1A). In response
68 regulators, C-terminal REC domains are fused to a broad range of N-terminal effector domains,
69 and predominantly function as transcription regulators (Figure 1B). Previous structural and
70 biochemical studies of the REC protein family showed that variable amino acid sequences in
71 active-site adjacent alpha-helices that from the interaction interface determine specificity with
72 cognate histidine kinases to mediate highly specific, context dependent, phosphotransfer to the

73 active-site aspartate residue (Varughese et al. 1998; Stock et al. 2000; Casino et al. 2009; Papon
74 and Stock 2019).

75 How the REC protein family evolves is of interest due to their ubiquitous role in cellular
76 signaling and regulation of cellular function. In the evolution of bacterial two-component systems,
77 the interactions of cognate histidine kinases and response regulators are under negative purifying
78 selection, constrained by functional overlap between signaling systems that share sequence
79 identity at interaction interfaces (Siryaporn and Goulian 2008; Capra and Laub 2012; Capra et al.
80 2012; McClune and Laub 2020). Presumably, loss of a single two-component system, due to
81 gene-loss or growth in conditions that suppress two-component system activity, relaxes these
82 constraints, such that new two-component systems can sample the unused combinations of
83 amino acids sequences that code for the interaction interfaces (Capra et al. 2012). It has been
84 shown that while two-components sample new sequences, the phosphorelay function between
85 cognate kinase and regulators do not break, and phosphotransfer levels can be maintained during
86 the evolutionary process (Capra et al. 2010). This implies that REC protein family expansion
87 occurs by neutral drift (Ohta 2001) when evolutionary constraints are relaxed, but we still do not
88 understand if new combinations of sequences forming new interaction specificities are sampled
89 when these constraints remain intact (Figure 1C).

90 One challenge in understanding the evolution of large protein families is parsing
91 relationships between members of the protein family from amino acid sequences alone. Previous
92 studies (Pao and Saier 1995; Chen et al. 2004; Ashby and Houmard 2006) using phylogenetic
93 and clustering methods to parse molecular information from REC domains from species that span
94 short evolutionary distances (population of a species or species within a genera) showed that
95 members of the REC protein family resulted from independent gene-duplications, sharing a
96 common ancestor in bacterial history. Studies comparing domain architectures of REC domains
97 from extant species (Galperin 2005; Galperin 2010; Galperin 2018) suggest that REC domains
98 evolve vertically, passing the fused effector domains to daughter REC domains (Figure 1C). To

99 overcome the challenge in understanding how REC protein family expansion occurs over long
100 phylogenetic distances, we build upon insights from these previous studies, making use of the
101 over 200,000 sequenced bacterial genomes, to develop a method that can parse the evolution of
102 the sequenced REC domains in extant, sequenced species (Gumerov et al. 2020).

103 In this study, we ask whether neutral genetic drift alone or another evolutionary
104 mechanism can explain how new members of protein families emerge. Using an unsupervised
105 machine learning strategy, we explore the amino acid sequence landscape of the REC protein
106 family. We identify a subfamily of the REC protein family that emerged and expanded after a
107 within-gene-recombination event that changed the effector domain of this REC subfamily. We
108 show that functional discordance between parent and daughter signaling pathways, which
109 occurred after the within-gene-recombination event, gave rise to a new structural interface that
110 both facilitates phosphotransfer and prevents crosstalk.

111 **Results**

112 To understand how large protein families expand and evolve, we applied an unsupervised
113 machine learning (ML) algorithm that uses dimensional reduction to group similar domains based
114 entirely on the identities and positions of amino acids sequences in an alignment. We established
115 this strategy for large protein families, using the REC protein family (PF00072). To ensure diverse
116 sampling of REC domains across the bacterial clade, we randomly sampled bacterial genomes
117 from three taxonomic ranks, kingdom (Bacteria), phylum (Proteobacteria) and genera
118 (*Pseudomonas*), generating independent datasets of REC sequences. To control for misgrouping
119 due to gaps in the sequence alignments, we applied the algorithm to REC sequence alignments
120 with and without gap replacement by randomly generated amino acids. Using t-Distributed
121 Stochastic Neighbor Embedding algorithm(van der Maaten and Hinton 2008) with N principal
122 components to explain 95% of the variation in the sequences, we projected the dimensionally
123 reduced output of the ML algorithm in two-dimensions (Figures 1D,2, Supplemental Figures 1-3)
124 and color coded each REC domain (single point on the plot) with independent information about

125 the effector domain it is fused to in nature. The data structure of the REC protein family becomes
126 evident by highlighting the predominant effector domains that have transcriptional function, GerE,
127 Trans_reg_C and AAA+, noting that few differences in data structure were apparent between
128 REC sequences with and without gap replacement (Figures 1D, Supplemental Figure 1A). When
129 we applied the ML-algorithm to scrambled amino acid sequence alignments with gap
130 replacement, the REC domains appeared randomly distributed; however, REC domains with
131 scrambled sequences without gap replacement appeared to be arranged non-randomly
132 (Supplemental Figure 2). Determining that sequence ambiguity assigned by the hidden markov
133 model alignment strategy (Zhang and Wood 2003) can result in more ambiguous alignments for
134 REC amino acid sequences that share less sequence identity with the response regulators used
135 to build the REC consensus model (Pao and Saier 1995), we decided that sequences with gap
136 replacement would provide a data structure that was independent of the biases introduced by the
137 alignment strategy. To demonstrate consistency of the method, we repeated the random sampling
138 of REC sequences two more times and applied the strategy with gap replacement to each
139 sampling, each showing similar data structures to the first sampling (Supplemental Figure 1B,C).
140 Together these results validate this strategy, allowing us to infer from it the evolutionary history of
141 the REC protein family.

142 The REC protein family is divided into subfamilies, which we will call subclusters; each
143 REC sequence is represented by a point in the two-dimensional sequence landscape (Figures
144 1D,2, Supplemental Figures 1-3), and shares sequence identity with neighboring points.
145 Subclusters that are closer together tend to share the identity of their fused effector domains
146 (Figures 1B,C,D), indicating that the REC protein family evolved vertically, carrying effector
147 domain architectures through to the next generation (Figure 1C). The separation between
148 subclusters becomes more pronounced as we sample domains from lower taxonomic ranks
149 (kingdom, to phylum, to genera), suggesting that the domains are under negative purifying
150 selection. Based on the number of observed subclusters we can posit that despite evolutionary

151 constraints, the REC protein family has expanded over the course of bacterial evolution, but we
152 do not know whether protein families sample new combinations of amino acid sequences when
153 these constraints remain intact. We hypothesized that crosstalk (overlap in specificity) between
154 signaling pathways does not completely explain REC protein family expansion, because crosstalk
155 is fairly common and does not always result in loss in fitness. For diversifying selection to occur,
156 the signaling system would need to cause adverse effects on cellular function, such as those that
157 can result from within-gene-recombination (Ohta 1991; Björklund et al. 2005; Forslund et al. 2008;
158 Chan, Darling, et al. 2009; Chan, Beiko, et al. 2009; Forslund et al. 2019) (a subcategory of gene
159 conversion, also known as domain swapping or domain shuffling).

160 Within-gene-recombination has occurred many times throughout the evolution of the REC
161 protein family, and has been previously documented (Pao and Saier 1995; Stephenson and Hoch
162 2002; Chen et al. 2004; Qian et al. 2008). We chose to focus on the largest, most pronounced
163 instance of with-in-gene recombination in our dataset. This event can be visualized in the two-
164 dimensional sequence landscape by the presence of two major clusters of REC sequences with
165 GerE effector domains (colored in blue); the GerE cluster that lies near REC sequences with
166 AAA+ effectors (colored in red) is the product of a within-gene-recombination event that changed
167 the effector domain of a parent response regulator with a AAA+ effector to GerE (Pao and Saier
168 1995; Chen et al. 2004). We focus on this event for two reasons: (1) it is a clear example of protein
169 family expansion, given that the two distinct clusters of GerE fused response regulators are highly
170 visible in the two-dimensional sequence landscape; and (2) the recombination event is by default
171 linked to functional discordance, because AAA+ and GerE domains regulate transcription with
172 distinct sigma (σ) factors, σ70 and σ54, which are active in incompatible cellular contexts (Cases
173 et al. 2003; Potvin et al. 2008; Ronneau and Hallez 2019; Casas-Pastor et al. 2021).

174 To determine whether within-gene-recombination can lead to protein family expansion, we
175 needed to determine whether these proteins were under diversifying selection as a result of the
176 within-gene-recombination event. Using our unsupervised ML strategy, we were able to find that

177 the recombined response regulator likely emerged sometime in the proteobacteria lineage, based
178 on the presence of a second GerE subcluster in proteobacteria and its absence in other phyla
179 (Supplemental Figure 3A-B). More specifically, the GerE subcluster expanded in the subclades
180 of alpha, beta, and gammaproteobacteria (Figure 2, Supplemental Figure 3), but were not
181 observable in deltaproteobacteria. In the species tree-of-life (Hug et al. 2016),
182 alphaproteobacteria predates beta and gammaproteobacteria; we therefore reasoned that the
183 within-gene-recombination event had occurred sometime in the alphaproteobacteria lineage. This
184 insight enabled us repurpose the REC sequence landscapes to home in on the REC protein family
185 in alphaproteobacteria (Figure 2, Supplemental Figure 3C) and search for the REC sequences of
186 interest (Figure 3A) for detection of differential rates of evolution (Figure 3B, Supplemental Figure
187 4). We found that the within-gene-recombination event caused rapid (or episodic) diversifying
188 selection on the branch of response regulators that have GerE domains in extant species
189 (Supplemental Figure 4A). The consensus between the REC sequences of the parent and
190 recombined response regulators highlights the shared sequence identity between the parent REC
191 domains fused to AAA+ domains and recombined REC domains fused to GerE domains, apart
192 from two highly conserved residues, a leucine and a cysteine, in the recombined REC domains
193 fused to GerE domains (Figure 3C-D). We were also able to independently verify that these two
194 residues in the recombined REC domains fused to GerE domains were under positive selection,
195 using a method that identifies individual sites subject to episodic diversifying selection (Murrell et
196 al. 2012) (Supplemental Data 1). These results show that after the within-gene-recombination,
197 rapid selection occurred in the recombined regulators, however it does not explain the roles of
198 the leucine and cysteine residues in their functional context of mediating phosphotransfer from
199 their cognate kinases.

200 To understand how the leucine and cysteine residues shaped the expansion of the
201 recombined response regulators, we needed to probe their molecular roles in interaction and
202 specificity with their cognate kinases and their parent's cognate kinsases. However, the function

203 of these regulators, the input signals they respond to and the genes they regulate, were not known
204 before this study. We set out to determine those functions, by pursuing functional experiments in
205 *Pseudomonas putida* KT2440, which proved advantageous for several reasons (1) *Pseudomonas*
206 *putida* is a model organism in bioremediation and synthetic biology applications (Loeschcke and
207 Thies 2015; Jumper et al. 2021; Sharma et al. 2022); therefore, many genetics and functional
208 genomics experiments have been applied to understand this strain's broad metabolism, allowing
209 us to rapidly phenotype regulators to determine their functions; (2) *P. putida* KT2440 is a
210 gammaproteobacteria, and is among the species where we have identified the parent AAA+
211 response regulators and the recombined GerE response regulator (note that these regulators are
212 not present in *Escherichia coli)*. Two functional genomics screens were used to determine, (1)
213 the media conditions that cause randomly barcoded transposon insertions (RB-Tn) mutants at
214 positions of the response regulators to more grow slowly in a population of other RB-Tn mutants
215 (Supplemental Figure 5A); and (2) the genomic location of the DNA binding sites the response
216 regulators use to regulate transcription (Supplemental Figure 5B and supplemental description).
217 RB-Tn mutants of the response regulators showed growth phenotypes in defined media with
218 carboxylic acids as the sole carbon source and DNA binding sites were found upstream of genes
219 related to carboxylic acid assimilation; we therefore proposed that the regulators might respond
220 to carboxylic acids to transcriptionally regulate a set of genes involved in carboxylic acid
221 assimilation (Figure 4A). We validated these hypotheses with GFP reporter screens (Figure 4B,
222 Supplemental Figure 6A), finding that the recombined regulator in *P. putida* responds to butyrate
223 and regulates beta oxidation, while the parent regulator responds to glutamate and regulates
224 amino acid assimilation. The overlap in chemical structure between carboxylic acids (Figure 4A)
225 adds context of mis-signaling by chemical sensing to our proposed model for diversifying selection
226 of the highly conserved residues in the recombined regulator, but we needed to directly
227 investigate whether the evolved residues had a role in breaking interaction between the parent
228 and recombined regulators' signaling pathways.

229 The domain tree of the parent and recombined regulators in alphaproteobacteria revealed
230 that positive diversifying selection occurred after the emergence of the recombined regulator, but
231 also revealed that the parent regulator underwent a second and third duplication event after the
232 initial within-gene-recombination (Figure 3, Supplemental Figure 4). We did not detect instances
233 of episodic diversifying selection on these post-recombination, duplicated REC domain branches,
234 and thus determined they diverged from their parent REC domain by neutral genetic drift. From
235 the functional genomics experiments, we determined that these regulators are also regulated by
236 carboxylic acids and regulate carboxylic acid assimilation (Supplemental Figures 5,6A-B), raising
237 an important distinction between these regulators that duplicated after the recombination event
238 and the recombined regulators, despite the specificity overlap of sensing and responding to
239 carboxylic acids with the parent, the post-recombination duplicated regulators diverged by genetic
240 drift, they were not under negative purifying selection, nor positive diversifying selection. We
241 believe this observation strengthens our hypothesis that specificity overlap and crosstalk is not
242 disfavored, and that diversifying selection only occurs when the additional condition of functional
243 discordance is met.

244 To understand if functional discordance following with-in-gene recombination plays a role
245 in evolution in the REC protein family, we asked whether the identified mutations in the
246 recombined regulator: (1) enables it to interact specifically with its cognate kinase; and (2) protects
247 it from crosstalk with its parent regulator's cognate kinase. To answer these questions, we applied
248 a specificity-switching assay, in which we switched the six residues that tend to co-vary with
249 cognate kinases across *Pseudomonads* (Supplemental Figure 7); the list of six residues included
250 the conserved leucine residue, but excluded the conserved cysteine residue (Figure 4C-H). We
251 found that the changes to the sequence of PP_1066, the parent regulator, were sufficient to switch
252 its specificity to the recombined regulator's cognate kinase (Figure 4I), however the same
253 mutations were not sufficient to switch the specificity of PP_3551, the recombined regulator
254 (Figure 4J). We hypothesized that the capability to switch by PP_1066, and inability to switch by

255 PP_3551 was intrinsic to the role of the leucine and cysteine residues in regulating specificity and
256 cros-talk.

257 To understand the physical role of leucine and cysteine in PP_3551 in connection to the
258 observed trends in the specificity-switching experiment, we turned to the structural prediction of
259 PP_3551, PP_1066, and their respective mutants determined by AlphaFold (Jumper et al. 2021).
260 In PP_3551, the conserved leucine residue (Figure 4E-F, Supplemental Figure 8) sits inside of
261 the alpha helix that canonically interacts directly with its cognate kinase. We can infer that when
262 we switched PP_1066 with covarying residues from PP_3551, we encoded the new specificity,
263 and enabled PP_1066 to interact with the cognate kinase of PP_3551 (Figure 4I), showing that
264 the new interface is responsible for the interaction of PP_3551 with its cognate kinase. On the
265 other hand, the cysteine residue lies within the same beta-sheet as the active aspartate residue
266 that is canonically phosphorylated by a cognate kinase (Figure 4G-H). When we switched the
267 residues of PP_3551 we left the cysteine residue intact, because it was not among the six
268 covarying residues. The specificity switch PP_3551 mutant's interaction site is almost identical to
269 PP_1066 with the key difference being this cysteine residue. Because the specificity switched
270 PP_3551 mutant did not interact with the cognate kinase of PP_1066 (Figure 4J), we reasoned
271 that the cysteine residue may be responsible for preventing crosstalk with its parent, however
272 further studies are need to reinforce this hypothesis. Therefore, the leucine residue plays a role
273 in making contact with the cognate kinase of the recombined regulator, facilitating
274 phosphotransfer, while we expect the cysteine residue plays a role in protecting the recombined
275 regulator from interaction with the recombined regulator's parent's cognate kinase. Here we show
276 that positive selection occurred after the within-gene-recombination event, forging new
277 mechanisms of interaction specificity and protection against crosstalk.

278 **Discussion**

279 The REC protein family undergoes three mechanisms of evolution, neutral genetic drift,
280 negative purifying selection, and as determined by this study, positive diversifying selection

281 (Figure 5A,B). Prior to this study, it was understood that neutral drift occurs when crosstalk
282 between functionally overlapping signaling systems does not affect cellular fitness (Siryaporn and
283 Goulian 2008; Groban et al. 2009; Capra et al. 2010; Siryaporn et al. 2010; Haushalter et al.
284 2015). It was also established that negative selection occurs when overlap in specificity between
285 signaling systems results in dysregulation of cellular function affecting cellular fitness (Capra et
286 al. 2012). This study demonstrates that REC protein family expansion can occur by positive
287 diversifying selection, and has occurred in a test case, in which a new signaling system emerged
288 by within-gene-recombination and functional overlap between the old and new signaling systems
289 affected cellular fitness. Specifically, our results show that a within-gene-recombination in a
290 duplicated response regulator of carbon assimilation changed the context in which this new
291 regulator performed its transcriptional function (changing the effector domain from its parent
292 regulator's σ54 dependent transcription to σ70 dependent transcription). We show that specificity
293 and functional overlap between the recombined response regulator and its parent gave rise to
294 two new mutations in the recombined response regulator that form a new interface of interaction
295 and prevents crosstalk with its parent response regulator (Figure 5A) by rapid diversifying
296 selection.

297 In this study we applied an unsupervised machine learning strategy to study the protein
298 sequence landscape of the REC protein family. One of the benefits of this strategy, over
299 previously applied strategies(Pao and Saier 1995; Chen et al. 2004; Ashby and Houmard 2006;
300 Forslund et al. 2008; Forslund et al. 2019), is that it enabled us to characterize the relationship
301 between REC protein family members over long evolutionary distances. The alternative approach
302 of inferring evolution of a large protein family across long phylogenetic distances from a domain
303 tree typically results in long branch distances, and uncertainty of branch positions (Efron et al.
304 1996; Simon 2022). For this reason, it is challenging to build reliable domain trees for large protein
305 families, specifically the REC protein family, which we estimate has between 10-100 million
306 members in sequenced bacteria (Gumerov et al. 2020). We overcame this challenge by

307 repurposing the ML strategy to find closely related REC domains over a defined evolutionary
308 distance (Figure 3A), after which we could build a reliable domain tree (Figure 3B) and apply
309 methods to detect differential rates of evolution (Supplementary Figure 4A). One pitfall of the ML
310 strategy is that the points on resultant maps do not maintain their positions for the same datasets
311 between runs, however the relative position of the points for the same datasets are maintained
312 between runs (van der Maaten and Hinton 2008)). Further development of this strategy,
313 specifically implementing a bootstrapping method, will enhance the overall reliability in its
314 application to the REC and other protein families. This tool will also be useful for distinguishing
315 the relationships between orthologous and paralogous response regulators (or other large protein
316 families) across species of interest.

317 Based on this study, we propose that diversifying selection in the REC protein family
318 occurs when two conditions are met: (1) overlap in specificity between signaling cascades (for
319 signals or interaction interfaces); and (2) the outcome of the regulation negatively impacts cellular
320 fitness. Results from this study and others (Siryaporn and Goulian 2008; Groban et al. 2009;
321 Capra et al. 2010; Noriega et al. 2010; Siryaporn et al. 2010; McClune et al. 2019) suggest that
322 functional overlap between two-component systems that occur after duplication does not always
323 result in negative purifying selection (Figure 5B). Specifically, in our study, we found that the
324 parent response regulator duplicated and diverged a second and third time after the selection of
325 the recombined regulator (Figure 3B, Supplemental Figure 4). Although these new regulators
326 were presumably subjected to an inherent overlap in specificity and function with the parent
327 regulator as they sampled sequences in their trajectory to new specificity, we determined they
328 were not under positive diversifying selection, providing additional evidence that overlap in
329 specificity can be tolerated by the cell (Figure 5B). The recombined regulator had comparable
330 overlap in specificity with its parent regulator to these other duplicated response regulators - then
331 why did the recombined regulators and regulators that duplicated and diverged after the
332 recombination show different rates of evolution? After the within-gene-recombination changed the

333 effector domain from its parent regulator's σ54 dependent transcription to σ70 dependent
334 transcription the recombined and parent response regulators regulated their overlapping function
335 under the incompatible regulatory contexts of σ54 and σ70 (Cases et al. 2003; Potvin et al. 2008;
336 Ronneau and Hallez 2019; Casas-Pastor et al. 2021). Although we cannot rule out the possibility
337 that diversifying selection occurred for a different reason, the simplest explanation for the
338 evolution of the recombined response regulator, is that differences in regulation by the sigma
339 factors negatively impacted cellular fitness, and were the source of the functional discordance
340 that gave rise to the selected mutations in the recombined regulator (Figure 5A).

341 This study establishes positive diversifying selection as a mechanism of the evolution for
342 the REC protein family, however future studies are needed to determine the role of the selected
343 cysteine residue in the recombined regulator. Our results show the conserved cysteine residue
344 was positively selected (Figure 3), and experimental results allow us to speculate that this residue
345 prevents interaction between the recombined regulator and its parent regulator, however,
346 because we rely on the negative result that PP_3551 could not switch its specificity (Figure 4J),
347 these experiments do not definitively confirm this hypothesis. Future studies are needed to
348 confirm whether the conserved cysteine residue prevents crosstalk.

349 In our model for diversifying selection of a test case in the REC protein family, duplication
350 followed by recombination led to an overlap in signals and outputs under competing regulatory
351 contexts giving rise to residues that facilitate a new interaction and prevent crosstalk. We propose
352 that diversifying selection is a mechanism of evolution for large protein family expansion if
353 conditions of functional discordance are met, showing that within-gene-recombination can
354 facilitate such conditions. In comparison to expansion in protein families where evolution is directly
355 influenced by an immediate requirement; examples being dynamic environmental factors that
356 need response in immune systems proteins (e.g. toxin-antitoxin (Jurėnas et al. 2022); Ig (Gaebler
357 et al. 2021)) or small molecule sensing protein families (e.g. GPCRs/olfactory receptors
358 (Bargmann 2006; Vandewege et al. 2016); efflux pumps (Henderson et al. 2021), the REC protein

359 family is a midpoint in signaling cascades and immediate fitness or “arms race” factors may not
360 be expected not influence its expansion. However, our study indicates that even for this class of
361 large protein families positive selection occurs, not by changing environmental conditions - as we
362 might have predicted - but instead due to genetic perturbations like recombination events. It
363 should be noted that although recombination can be a source for functional discordance, as it is
364 in this study’s test case, recombination can be neutral and will not always result in functional
365 discordance. Further exploration of the REC sequence landscape or the sequence landscape of
366 other protein families may elucidate whether other genetic perturbations create conditions for
367 diversifying selection when evolutionary constraints remain intact. It will also be interesting to
368 understand whether there are limitations on protein family expansion that occurs by neutral drift,
369 even when evolutionary constraints are lifted. Overall, this study shows that positive diversifying
370 selection is a mechanism in the expansion of the REC protein family and that it occurs by
371 functional discordance. We believe this result is significant in understanding the evolution of the
372 REC protein family, which directly modulates a vast range of cellular functions. This knowledge
373 provides important context for assessing their role in microbial function, microbial communities
374 and in engineering efforts in biosystems design and synthetic biology applications.

375 **Figure Legends**

376 ***Figure 1: Functional context for insight into the evolution of the REC protein family.***
377 (A) REC protein family in the context of bacterial two-component systems: Membrane bound
378 histidine kinases sense a signal, autophosphorylate, and phosphorylate, with precise biochemical
379 specificity, a cognate response regulator. The phosphorylated cognate response regulator goes
380 on to regulate cellular functions, including transcription, chemotaxis, or other functions.
381 (B) Domain architecture of the two-component system (shown in A). The histidine kinases’ sensor,
382 dimerization and histidine phosphotransfer (DHp), and catalytic (CA) domains coordinate the
383 initial autophosphorylation in the two-component signaling cascade. The signal is transmitted by
384 phosphotransfer to the cognate response regulators’ receiver (REC) domain (bolded oval). The

385 effector domain (oval labeled “E”), completes the signaling cascade. Effector domains “E” are
386 mostly DNA binding and the most abundant are Trans_reg_C (yellow) , GerE (blue), AAA+ (red),
387 and HTH_8 (green). Because HTH_8 domains often co-occur with AAA+ they are shown as
388 overlapping red and green ovals - for simplicity, AAA+-HTH_8 domains are called AAA+ domains
389 throughout the text. Effector domains with non-DNA binding function are shown as CheY (gray),
390 other (white), and no domains (black). The effector domain color coding shown in this figure is
391 used for all subsequent figures.
392 (C) Model of the evolution of the REC protein family shown as a tree. We assume all REC domains
393 share a common ancestor and that REC domains fused to the same effector domains are more
394 closely related to one another than REC domains fused to different effector domains, showing
395 regulators with distinct domain architectures and colors (refer to 1B) at the tips of the tree with
396 coalescent branches. We know that genetic drift has occurred in the evolutionary history of the
397 REC protein family when evolutionary constraints are relaxed, however, we do not know what
398 causes REC domains to sample new combinations of sequences that encode new specificities
399 when these constraints are intact.
400 (D) Output from the dimensional reduction algorithm assesses the similarity between members of
401 the REC protein family in Bacteria (leftmost panel), Proteobacteria (middle panel), and
402 Pseudomonas (right panel) species, showing the relationship between REC domain sequence
403 alignments with gap replacement and explaining 95% of the variation between the sequences.
404 The REC domains were sampled from species found within the taxonomic rank (kingdom -
405 Bacteria, phylum-Proteobacteria, or genera-Pseudomonas) labeled at the top of each plot. To
406 control for overrepresentation of subclades due to more representative species with full genome
407 sequences in any given subclade, species were sampled evenly from the taxonomic rank below
408 the one represented in the plot title (e.g. The taxonomic rank below kingdom is phylum; the
409 maximum of species from each bacterial phylum were randomly sampled to generate the bacteria
410 dataset (see Table S1)). After species sampling, we identified all proteins with REC domains in

411 each of the sampled species' genomes and aligned their sequences. To read the plot, each point
412 represents the sequence of a REC domain from the sampled genomes, points that are close
413 together share sequence identity with each other. Each REC domain is annotated by the identity
414 of its effector domain Trans_reg_C (yellow) , GerE (blue), AAA+ (red), CheY (gray), other (gray
415 outline), and no domains (black). Note that the location of REC domains is not fixed in the plot
416 between independent runs of the algorithm, however, the relative distribution between the points
417 is visually consistent between runs. The within-gene-recombination that changed parent REC
418 domain fused to AAA+ domain to REC domain fused to GerE domain is apparent by the presence
419 of two distinct blue clusters: the GerE cluster (blue) found close to the AAA+ cluster (red) resulted
420 from within-gene-recombination of effector domains and is indicated by a black arrow.

421 ***Figure 2: Within-gene-recombination that changed parent REC domain fused to AAA+***
422 ***domain to REC domain fused to GerE domain occurred during the Alphaproteobacteria***
423 ***lineage.***

424 Output from the machine learning algorithm assesses the similarity between members of the REC
425 protein family in (from left to right) Alphaproteobacteria, Betaproteobacteria,
426 Gammaproteobacteria, Deltaproteobacteria species, showing the relationship between REC
427 domain sequence alignments with gap replacement and explaining 95% of the variation between
428 the sequences. The REC domains were sampled from species found within the taxonomic rank
429 (class) labeled at the top of each plot. To control for overrepresentation of subclades due to more
430 representative species with full genome sequences in any given subclade, species were sampled
431 evenly from the taxonomic rank below the one represented in the plot title (e.g. the taxonomic
432 rank below class is order; the maximum of species from each bacterial phylum were randomly
433 sampled to generate the bacteria dataset (see Table S1)). After species sampling, we identified
434 all proteins with REC domains in each of the sampled species' genomes and aligned their
435 sequences. To read the plot, each point represents the sequence of a REC domain from the
436 sampled genomes, points that are close together share sequence identity with each other. Each

437 REC domain is annotated by the identity of its effector domain Trans_reg_C (yellow) , GerE (blue),
438 AAA+ (red), CheY (gray), other (gray outline), and no domains (black). Note that the location of
439 REC domains is not fixed in the plot between independent runs of the algorithm, however, the
440 relative distribution between the points is visually consistent between runs. The within-gene-
441 recombination that changed parent REC domain fused to AAA+ domain to REC domain fused to
442 GerE domain is apparent by the presence of two distinct blue clusters: the GerE cluster (blue)
443 found close to the AAA+ cluster (red) resulted from within-gene-recombination of effector domains
444 and is indicated by a black arrow.

445 ***Figure 3: Episodic diversifying selection in the REC domain occurred after within-gene-***
446 ***recombination that changed parent REC domain fused to AAA+ domain to REC domain***
447 ***fused to GerE domain***

448 (A) Output from the machine learning algorithm assesses the similarity between members of the
449 REC protein family in Alphaproteobacteria species (circles) and *Pseudomonas putida* KT2440
450 (x's). The sampled Alphaproteobacteria species are the same as those in Figure 2 (left-most
451 panel); note that the location of REC domains is not fixed between independent runs of the
452 algorithm, however, the relative distribution between the points is consistent between runs. The
453 within-gene-recombination, which is apparent in Alphaproteobacteria by the presence of two
454 distinct blue clusters: the GerE cluster (blue) found close to the AAA+ cluster (red) resulted from
455 within-gene-recombination of effector domains, is indicated by a black box. The zoom panel of
456 the black box shows the protein names of the REC domains within the box that are closely related
457 to each other and have undergone a within-gene-recombination that switched effector domains.
458 (B) The REC domains within the black box (Figure 3A) from alphaproteobacteria species (circles)
459 are used to construct a domain tree. The DNA sequences of the REC domains were aligned with
460 MAFFT. Using GCF_000169415-SSE37_RS08100 as an outgroup, we built the representative
461 domain tree with iqtree, and annotated the branch colors red if the domain's effector identity was
462 AAA+ or blue if the domain's effector identity was GerE (or no domain). Bootstrap supports are

463 labeled at the nodes and shown as branch thickness. We independently determined that the
464 recombined REC domains with GerE (or no domain) effectors were under episodic diversifying
465 selection. The domain tree also shows that the parent REC domains with AAA+ effectors (red)
466 independently duplicated and diverged after the within-gene-recombination.
467 (C, D) The strategy applied to find the REC domains within the box (Figure 3A) was applied to a
468 find parent REC domains with AAA+ effectors and recombined REC domains with GerE (or no
469 domain) effectors for more Alphaproteobacteria species (C) and Proteobacteria species (D). The
470 amino acid sequences of the REC domains were aligned with MAFFT and separated in two
471 distinct groups (AAA+ or GerE) based on the identity of their effector domains. The alignments of
472 each group were used to generate WebLogo consensus motifs revealing two residues, leucine
473 and cysteine (in this alignment, L16 and C54 - highlighted with red background and red star
474 below), are conserved in the GerE groups. Sequence alignments of AAA+ groups show the parent
475 REC domains differ at alignment residue 16 having either alanine, tryptophan, or threonine at that
476 position
477 ***Figure 4: Parent and recombined response regulators in P. Putida KT2440 are regulators***
478 ***of carbon assimilation and evolved by episodic diversifying selection to break an overlap***
479 ***in specificity.***
480 (A) Model of regulation of carboxylic acids in *P. putida* KT2440 by the parent (PP1066) and
481 recombined (PP3551) response regulators determined by functional genomics experiments.The
482 parent two-component system (PP1067/PP1066), colored in red is activated by glutamate, and
483 regulates genes for glutamate assimilation with AAA+ dependent σ54 transcription machinery.
484 The recombined two-component system (PP3552/PP3551), also colored in red, is activated by
485 butyrate, and regulates genes for beta oxidation with GerE dependent σ70 transcription
486 machinery (the recombined GerE domain is colored blue). Based on the presence of
487 transmembrane or sensing domains in the histidine kinases, we model PP1067 as membrane
488 bound with a dCache domain for sensing glutamate, and PP3351 as cytosolic with two PAS

489 domains for sensing butyrate. The residues in PP3551 REC domain under diversifying selection
490 are represented by black stars on the PP3551 REC domain. Chemical similarity between
491 glutamate and butyrate, which provides functional context to the proposed mechanism of
492 functional discordance that caused diversifying selection, is shown in a box at the top right
493 (B) *P. putida* KT2440 transformed with a GFP reporter plasmid for regulation by PP1066 or
494 PP3551 were grown in defined glucose media with or without (white) glutamic acid (red) or butyric
495 acid (blue). Top panel shows the reporter plasmid for PP1066 is upregulated when grown with
496 glutamic acid and the reporter plasmid for PP3551 is upregulated when grown with butyric acid.
497 Bottom panel shows reporters for PP1066 and PP3551 are respectively not activated if the
498 regulators, PP1066 or PP3551 are deleted from the genome. Center line, median; box limits,
499 upper and lower quartiles; whiskers, 1.5x interquartile range; points with black diamonds, outliers;
500 n = 3.
501 (C) The same strategy that was applied to find the REC domains within the black box (Figure 3A)
502 was applied to find parent REC domains with AAA+ effectors and recombined REC domains with
503 GerE (or no domain) effectors for Gammaproteobacteria species. The amino acid sequences of
504 the REC domains were aligned with MAFFT and separated in two distinct groups (AAA+ or GerE)
505 based on the identity of their effector domains. The alignments of each group were used to
506 generate WebLogo consensus motifs, which revealed that two residues, leucine and cysteine (in
507 this alignments, L16 and C52 - highlighted with red background and red star below), are
508 conserved in the GerE groups. The 6 residues in the REC domain that tend to covary in
509 Pseudomonas species are highlighted with blue background and blue triangle below, noting that
510 L16 is both covariant and selected, while C52 is only selected. Sequence alignments here and in
511 Figure 3C,D show the parent REC domains differ at alignment residue 16 having either alanine
512 (PP1066: the parent regulator), tryptophan (PP1401), or threonine (PP0263) at that position.
513 (D) Alignment of PP1066 and PP3551 REC domains. Covariant (blue), selected (yellow),
514 covariant and selected (red), active aspartate (purple) residues are highlighted by the indicated

515 background color. PP1066* and PP3551* match the sequence of PP1066 and PP3551,
516 respectively, but are switched at the covariant positions (blue). These sequences test whether
517 the specificity of PP1066 and PP3551 can be switched.
518 (E,F,G,H) To show the structural impact of specificity switching, we modeled the structure of
519 PP3551 (E), PP1066* (F), PP1066 (G), PP3551*(H) with the structural prediction of the full length
520 protein using AlphaFold. Covariant (blue), selected (yellow), covariant and selected (red), active
521 aspartate (purple) residues are highlighted. The covariant residues in PP3551 (E), including the
522 selected leucine residue L16, is coded in PP1066* (F), the selected cysteine residue (C52)
523 colored yellow is not. PP3551* is coded with specificity determining residues of PP1066, replacing
524 selected leucine and covariant residue with alanine (L16A), but maintains its selected but not
525 covariant cysteine residue (C52).
526 (I) P. putida KT2440 ΔPP1066ΔPP3551 transformed with a GFP reporter plasmid for regulation
527 by response regulators (RR) PP3551 and PP1066* were grown in defined glucose media with or
528 without (white) glutamic acid (red) or butyric acid (blue). Percent arabinose (% ara) used to induce
529 expression of heterologous response regulators and whether the respective cognate histidine
530 kinases (ΔHK) are deleted from the genome is indicated below the plot. Center line, median; box
531 limits, upper and lower quartiles; whiskers, 1.5x interquartile range; points with black diamonds,
532 outliers; n = 6.
533 (J) P. putida KT2440 ΔPP1066ΔPP3551 transformed with a GFP reporter plasmid for regulation
534 by response regulators (RR) PP1066 and PP3551* were grown in defined glucose media with or
535 without (white) glutamic acid (red) or butyric acid (blue). Percent arabinose (% ara) used to induce
536 expression of heterologous response regulators and whether the respective cognate histidine
537 kinases (ΔHK) are deleted from the genome is indicated below the plot. Center line, median; box
538 limits, upper and lower quartiles; whiskers, 1.5x interquartile range; points with black diamonds,
539 outliers; n = 6.
540 ***Figure 5: Models of the evolution of the REC protein family***

541 (A) Model of the evolution of the REC protein family shown as a tree, updated by this study. We
542 assume all REC domains share a common ancestor and that REC domains fused to the same
543 effector domains evolved vertically, showing regulators with distinct domain architectures and
544 colors (refer to 1B) at the tips of the tree with coalescent branches. Note that the order of events
545 in steps 1-3 are uncertain. We model the findings of this study that diversifying selection and
546 sequence divergence occurred after the within-gene-recombination that changed a parent REC
547 domain fused to AAA+ domain to a recombined REC domain fused to a GerE domain. Because
548 we determined that the parent and recombined REC domains regulate similar cellular responses
549 and the recombined REC domains activate transcription under a new sigma factor regulatory
550 contexts, we propose functional discordance gave rise to episodic diversifying selection, changing
551 the interaction specificity and preventing the recombined REC domain from activating unwanted
552 cellular responses that result from crosstalk. Changes that have broad cellular consequences,
553 specifically those that cause functional discordance between members of large protein families
554 can give rise to diversifying selection and lead to protein family expansion.
555 (B) Models of the evolution of the REC protein family in a sequence-fitness landscape. Top and
556 bottom panels show the sequence-fitness landscape as projections of sequence and fitness. The
557 top panes show the x,y, plane representing the available combinations of amino acid sequences
558 to the REC protein family, where z is the fitness (or distribution of REC domains with amino acid
559 sequences defined by the x,y plane). If the fitness of a domain is high, it is shown as a solid black
560 point on the plot, the boundaries of the fitness (or possible combinations of amino acid sequences
561 that allow the domain to maintain its specificity) for the domains that are colored in red, yellow,
562 orange, or blue are shown as a gray radius. Pointed arrows show the direction of positive selection
563 or neutral drift, blunted arrows show the direction of negative selection. The bottom panes show
564 the fitness as a function of the cross-section in the x,y plane (f(x,y)) (dashed line in the top panel)
565 of the domain that are colored red, yellow, orange, or blue. Each column shows a different mode
566 of evolution discussed in this report (from left to right: purifying selection, genetic drift, genetic drift

567 under purifying selection, and episodic diversifying selection). Purifying selection selects against
568 new REC domains that interfere with the specificity and function of existing REC domains. Genetic
569 drift occurs when constraints in the sequence landscape are relaxed due to loss or suppressed
570 activity of other REC domains that would otherwise constrain REC protein family expansion.
571 Genetic drift under purifying selection can be tolerated when overlap in sequence specificity is
572 not disadvantageous for the species in which the new sequence arises, however, this study shows
573 that episodic diversifying selection occurs when the overlap in sequence specificity leads to
574 functional discordance.
575

576 **Methods**

577 **Two-dimensional visualization of protein family sequences**

578 *Sampling Genomes and creating REC domain databases*

579 Databases of REC domains (PF00072) that were used to make all REC sequence landscapes
580 were sampled from the microbial signal transduction database (MISTDB) (Gumerov et al. 2020)
581 - a curated database of the signal transduction genes from over 200,000 bacterial genomes -
582 using their API and custom functions written in python. To control for bias driven by genome
583 availability for species of various taxonomic ranks (e.g gammaproteobacteria more represented
584 than any other class in the proteobacteria phylum) we took a subset of the available data by
585 randomly sampling species based on taxonomic rank (e.g. the taxonomic rank below kingdom is
586 phylum; the maximum of species from each bacterial phylum were randomly sampled to generate
587 the bacteria dataset (Table S1)). The following datasets were forced to include *P. putida* KT2440,
588 which we used to track the parent and recombined regulator in the two-dimensional projections
589 of the REC domains: Bacteria, Proteobacteria, *Pseudomonas*, and Alphaproteobacteria in Figure
590 3A. Again, using the MISTDB API, we used a custom function to generate a second database of
591 all of the amino acid sequences of two-component system genes from the sampled species, while
592 keeping a record of each protein's metadata (e.g. fused domains). We then sampled this database

593 to find all response regulators and their respective sequences to generate fasta files that include
594 entries for each response regulator in the database.

595 *REC domain alignments*

596 We aligned the REC domain entries in the generated fasta files from the REC domain sampling
597 functions using hmmalign (Zhang and Wood 2003; Finn et al. 2011) to the REC pfam consensus
598 motif, PF00072 (Pao and Saier 1995). Using a custom python function, we linked the aligned
599 domain back to its metadata in the REC domain database. When gap replacement was applied,
600 gaps were replaced by a randomly generated amino acid. To generate scrambled datasets, we
601 scrambled the individual sequences using a custom function that randomly samples residues and
602 rejoins them in a new order while maintaining the original length of the alignment.

603 *Projection of REC domain alignment variability in two-dimensional space*

604 We then encoded the sequences into a discrete variable vector representation(Jing et al. 2020),
605 by encoding each amino acid into a 21-dimensional zero vector (one dimension for each possible
606 amino acid and a gap character), except for the index representing the amino acid, which is set
607 to one. Each Lx21-dimensional matrix, where L is the length of the aligned protein sequence, is
608 flattened to a Lx21-length vector. Each vector representing the alignment of a single protein
609 sequence is stacked into a Nx(Lx21) matrix and dimensionally reduced to N dimensions to explain
610 95% of the variation by principal component analysis in the data before being reduced to Nx2
611 dimensions using the t-Distributed Stochastic Neighbor Embedding algorithm(van der Maaten
612 and Hinton 2008). We approximated the perplexity, or the expected size of the clusters, as the
613 number of clades in the taxonomic rank below the highest taxonomic rank queried (e.g. if we were
614 looking at a kingdom rank, the next clade down is the phyla. The perplexity is then equal to the
615 number of unique phyla in the dataset - see Table S2 (unique taxa in rank below).) Note that we
616 found a binary encoding was sufficient for our use case, but another encoding may be more
617 suitable for other large protein families.

618 Source code and data are available at https://github.com/mgarber21/Large_Protein_Families.git

619 ***Isolating the parent and recombined regulators from randomly sampled REC domains in***
620 ***Alphaproteobacteria, Gammaproteobacteria, or Proteobacteria species***
621 Using *P. putida* KT2440 to track the parent and recombined regulator in the two-dimensional
622 projections of the REC domains in Alphaproteobacteria, Gammaproteobacteria, or Proteobacteria
623 species, we defined boundaries in the projection and to isolate the candidate proteins. Using the
624 DNA or amino acid sequences, we aligned the candidate domains (isolating the REC domain
625 from the protein or protein coding sequence) using the MAFFT-LINSI algorithm from MAFFT
626 v7.310(Katoh and Standley 2013)**.** We then used IQTREE (Nguyen et al. 2015) to build the
627 Alphaproteobacteria REC domain tree, using the aligned DNA sequences of the REC domains
628 with a transversion model, empirical base frequencies, and discrete Gamma model
629 (TVM+F+I+G4), also using outgroup species, GCF_000169415-1-SSE37_RS08100, and 1000
630 bootstraps. Using these same sequences, we applied an adaptive branch site rel test for episodic
631 diversification, and detected individual sites subject to diversifying episodic selection using the
632 online aBSREL (Kosakovsky Pond et al. 2011; Smith et al. 2015) and MEME (Murrell et al. 2012)
633 tools from HyPhy in Datamonkey (Pond and Frost 2005; Delport et al. 2010; Weaver et al. 2018)
634 with default parameters and according to the user instructions. Logs and results can be found in
635 Supplemental Data 1. To generate amino acid consensus motif images for each subgroup, REC
636 domains fused to either AAA+ or GerE, excluding outgroup AAA+ domains, we binned the aligned
637 domains into their respective subgroups and generated a consensus motif using WebLogo
638 (Crooks et al. 2004).
639 **Fitness experiments using a library of randomly barcoded transposon insertion (RB-Tn)**
640 **mutants**
641 As described in prior reports(Thompson et al. 2019), the *P. putida* KT2440 RB-TnSeq library,
642 JBEI-1, was thawed, inoculated into 25 mL of LB medium supplemented with kanamycin, and
643 grown to OD_{600} of 0.5. Three 1 mL samples were taken after this step to serve as t_0 records of
644 barcode abundance. The library was then washed via centrifugation and resuspension in an equal

645 volume of MOPS minimal medium. The washed cells were then diluted 1:50 in MOPS minimal
646 medium with 10 mM L-glutamate serving as the sole carbon source. The library was cultured in a
647 96-well deep well plate sealed with a gas permeable membrane (VWR, USA). The plate was
648 shaken (700 rpm) in an INFORS HT Multitron (Infors USA Inc.) at 30 °C for 24 hrs. Duplicate 600
649 µL samples were then combined and BarSeq analysis was conducted as described
650 previously(Wetmore et al. 2015; Rand et al. 2017; Incha et al. 2020). Single carbon source fitness
651 data is available at http://fit.genomics.lbl.gov(Thompson et al. 2020).

652 **Automated DNA affinity purification with next generation sequencing (NGS)**

653 DNA preparation for NGS

654 Pseudomonas isolates were cultured in either LB or minimal media (see Table S3 for strain
655 specific minimal media recipes). Genomic DNA was purified with a promega wizard genomic
656 preparation kit (Promega, Madison, WI). DNA was sheared with covaris miniTUBE (Covaris,
657 Woburn, MA) to an average size of 200 bp. The DNA quality was confirmed by Bioanalyzer high
658 sensitivity DNA kit (Agilent, Santa Clara). Sheared DNA was then adapter-ligated (AL) with
659 NEBnext Ultra ii Library Preparation kit (New England Biolabs, Ipswich, MA). AL-DNA quality was
660 again confirmed by Bioanalyzer high sensitivity DNA kit (Agilent, Santa Clara). AL-DNA was
661 stored at -20 ˚C until required for downstream use.

662 *Expression Strain Design*

663 pet28 expression vectors with N-terminal 6x-His-tagged RRs were cloned by Gibson
664 assembly(Gibson et al. 2009). Plasmid design was facilitated by j5 DNA assembly design(Hillson
665 et al. 2012), see Table S4 for primers.

666 *Automated DNA affinity purification*

667 Quadruplicates of expression strains were grown in autoinduction media (Zyp-5052(Studier
668 2005)) at 37 ˚C, 250 RPM, for 5-6 hours and then transferred to grow at 17 ˚C, 250 RPM,
669 overnight. Cell pellets were harvested and lysed at 37 ˚C for 1 hour in a lysis buffer (1X TBS, 100
670 μM PMSF (Millipore Sigma, Burlington MA), 2.5 units/mL Benzonase nuclease (Millipore Sigma,
671 Burlington MA), 1 mg/mL Lysozyme (Millipore Sigma, Burlington MA)). Lysed cells were then
672 clarified by centrifugation at 3214 x g and further filtered in 96-well filter plates by centrifugation
673 at 1800 x g. To enable high-throughput processing, protein-DNA purification steps were
674 performed with IMAC resin pipette tips (PhyNexus, San Jose, CA) using a custom automated
675 platform with the Biomek FX liquid handler (Beckman Coulter, Indianapolis, IN). The expressed
676 RRs were individually bound to metal affinity resin embedded within the IMAC resin pipette tips
677 and washed in a wash buffer (1X TBS, 10 mM imidazole, 0.1% Tween 20). The bead bound RRs
678 were then mixed with 60 μL of DNA binding buffer (1X TBS, 10 mM magnesium chloride, 0.4
679 ng/μL AL-DNA, with or without 50 mM acetyl phosphate (split into duplicates)). The protein bound
680 to its target DNA was then enriched in an enrichment buffer (1X TBS, 10 mM imidazole, 0.1%
681 Tween 20) and eluted in an elution buffer (1X TBS, 180 mM imidazole). The elution was stored
682 at -20 ˚C for a minimum of one day and up to a week before proceeding to the NGS library
683 generation. See supplementary methods for detailed protocol.

684 *NGS Library Generation*

685 3.2 μL of the elution from the previous step was added to 3.5 μL SYBR green ssoAdvanced
686 (Biorad, Hercules, CA) and 0.15 μL of each dual indexed NGS primers. NGS libraries were
687 prepared by following the protocols for fluorescent amplification of NGS libraries(Chiniquy et al.
688 2020). Pooled libraries were sequenced by Illumina NovaSeq 6000 SP (100 cycles) (Illumina, San
689 Diego, CA).

690 *DAP-seq data analysis*

691 Sequenced reads were processed by a computational DAP-seq analysis pipeline as follows.
692 Adapters and low-quality bases were trimmed and reads shorter than 30 bp were filtered out using
693 Trimmomatic v.0.36(Bolger et al. 2014). The resulting reads were checked for contamination
694 using FOCUS (Silva et al. 2014). Then the reads were aligned to the corresponding
695 *Pseudomonas* spp. genome using Bowtie v1.1.2 (Langmead et al. 2009) with –m 1 parameter
696 (report reads with single alignment only). Resulting SAM files were converted to BAM format and
697 sorted using samtools v 0.1.19(Li et al. 2009). Peak calling was performed using SPP
698 1.16.0(Kharchenko et al. 2008) with false discovery rate threshold of 0.01 and MLE enrichment
699 ratio threshold of 4.0. Enriched motifs were discovered in genome fragments corresponding to
700 the peaks using MEME(Bailey et al. 2009) with parameters –mod anr –minw 12 –maxw 30 –
701 revcomp –pal –nmotifs 1. Source code of the DAP-seq analysis pipeline is available at
702 https://github.com/novichkov-lab/dap-seq-utils.

703 For conserved RRs with small numbers of high-confidence peaks (1-2 per genome), binding
704 motifs were predicted manually by a comparative genomics approach. Orthologous RRs were
705 identified by OrthoFinder2(Emms and Kelly 2019). For each of orthologous RRs, one genome
706 fragment corresponding to the peak with the highest enrichment value was selected for motif
707 search. Conserved motifs were discovered using the SignalX tool from the GenomeExplorer
708 package(Mironov et al. 2000) with the “inverted repeat” option.

709 **Co-variance analysis**

710 Cognate RRs and HKs from *Pseudomonas* and *E. coli* strains were identified as pairs if they were
711 found neighboring each other in their respective genomes. DHp (HisKA), CA (HATPase_C), and
712 REC (Response_reg) domain boundaries were determined with hmmsearch from HMMER
713 v3.1b2(Mistry et al. 2013). Fasta files of concatenated DHp-CA-REC domains from cognate and

714 randomized HK-RR pairs were aligned with the MAFFT-LINSI algorithm from MAFFT
715 v7.310(Katoh and Standley 2013). Alignment files were then queried for coevolution with the
716 ProDy *Evol* suite(Bakan et al. 2011; Bakan et al. 2014) in python and were plotted in a heatmap.
717 The highest scoring residues > 1.1 were used to inform hypotheses for specificity switch strains.

718 **GFP reporter strain generation and assays**

719 *Knockout strain generation*

720 1000bp homology fragments upstream and downstream of the target gene were cloned into
721 plasmid pKS18. Plasmids were then transformed into *E. coli* S17 and then mated into *P. putida*
722 via conjugation. Transconjugants were selected for on LB agar plates supplemented with 30
723 mg/ml kanamycin and 30 mg/ml chloramphenicol. Transconjugants were then grown overnight
724 on LB medium and were then plated on LB agar with no NaCl that was supplemented with 10%
725 (wt/vol) sucrose. Putative deletions were screened on LB agar with no NaCl supplemented with
726 10% (wt/vol) sucrose and LB agar plate with kanamycin. Colonies that grew in the presence of
727 sucrose but had no resistance to kanamycin were further tested via PCR with primers flanking
728 the target gene to confirm gene deletion.

729 *GFP reporter strains*

730 Promoter boundaries for p2453, p1400, p3553 were selected as the region just upstream of the
731 gene's start codon up until the start or stop codon of the next nearest gene. The promoters were
732 cloned upstream of the gene encoding sfGFP on a broad host range plasmid with BBR1 origin
733 and Kanamycin resistance, with Gibson cloning(Gibson et al. 2009). Primers in Table S4. The
734 plasmids were transformed into *P. putida* KT2440 or *P. putida* KT2440 mutant strains by
735 electroporation. Three biological replicates of each strain were cultured in LB and stored with 25%
736 (vol/vol) glycerol at -80 ˚C. Complementation plasmids (GFP reporter plasmids with full length RR
737 driven by pBAD promoter and constitutively expressed AraC) were combinatorially built

738 leveraging Golden Gate cloning(Engler et al. 2008) and j5 DNA assembly design(Hillson et al.
739 2012) (diva.jbei.org), primers in Table S4. The plasmids were transformed into gene knockout
740 strains of *P. putida* KT2440 by electroporation. 3-6 biological replicates of each strain were
741 cultured in LB and stored with 25 % (v/v) glycerol at -80 ˚C.

742 *RRs with switched specificity*

743 Gene blocks (TWIST Biosciences, San Francisco, CA) of REC domains (Table S3) with co-
744 varying mutations (co-variation score > 1.1 - see supplemental figure 7) were cloned into the
745 complementation plasmids with Gibson assembly(Gibson et al. 2009). The plasmids were
746 transformed into *P. putida* KT2440 or knockout strains of *P. putida* KT2440 by electroporation.
747 Six biological replicates of each strain were cultured in LB and stored with 25 % (vol/vol) glycerol
748 at -80 ˚C.

749 *GFP reporter Assays*

750 Reporter strains were adapted to M9 minimal media (MM) (see supplemental methods for strain
751 specific minimal media recipes) supplemented with 0.5 % (wt/vol) glucose as the sole carbon
752 source in 3 overnight passages, and stored in MM at -80 ˚C in 25 % (vol/vol) glycerol. Adapted
753 strains were cultured in MM + 0.5 % (wt/vol) glucose and passaged to MM + 0.5 % (wt/vol) glucose
754 with or without a second carbon-source (40 mM glutamic acid, 40 mM a-ketoglutaric acid, or 20
755 mM butyric acid, unless otherwise specified). Note that specificity switch strains have response
756 regulators under pBAD promoters, which were first calibrated with 2-fold dose response of
757 arabinose concentrations between 0-0.1% (Supplemental Figure 9). After 24-hours of growth,
758 samples were diluted 1:100 in 1X PBS, and fluorescence was measured by flow cytometry on the
759 BD Accuri C6 (BD Biosciences, San Jose, CA). Autofluorescence was gated out with FlowJo (BD
760 Biosciences, San Jose, CA), using a non-fluorescent strain of *P. putida* KT2440 carrying an empty
761 vector for reference (Supplemental Figure 10). To remove noise, the GFP mean for samples with

762 less than 150 events after gating was set to 0. Otherwise, the GFP mean of the remaining events
763 after gating was reported.

764 **AlphaFold predictions of wildtype and mutant response regulators**

765 Full length amino acid sequences of wildtype PP_1066, and the respective specificity switching
766 mutants of PP_3551 and PP_1066 were queried using ColabFold by AlphaFold (Jumper et al.
767 2021) using the default parameters.PDB files and prediction logs can be found Supplemental
768 Data 2. The structural prediction of PP_3551 was retrieved from the AlphaFold deepmind
769 database (Varadi et al. 2022). The pdb file from each protein's highest ranking structure from
770 AlphaFold was then visualized and annotated with Chimera X (Pettersen et al. 2021).

771

772 References

773 Ashby MK, Houmard J. 2006. Cyanobacterial two-component proteins: structure, diversity,
774 distribution, and evolution. Microbiol. Mol. Biol. Rev. 70:472–509.

775 Bailey TL, Boden M, Buske FA, Frith M, Grant CE, Clementi L, Ren J, Li WW, Noble WS. 2009.
776 MEME SUITE: tools for motif discovery and searching. Nucleic Acids Res. 37:W202-8.

777 Bakan A, Dutta A, Mao W, Liu Y, Chennubhotla C, Lezon TR, Bahar I. 2014. Evol and ProDy for
778 bridging protein sequence evolution and structural dynamics. Bioinformatics 30:2681–2683.

779 Bakan A, Meireles LM, Bahar I. 2011. ProDy: protein dynamics inferred from theory and
780 experiments. Bioinformatics 27:1575–1577.

781 Bargmann CI. 2006. Comparative chemosensation from receptors to ecology. Nature 444:295–
782 301.

783 Björklund AK, Ekman D, Light S, Frey-Skött J, Elofsson A. 2005. Domain rearrangements in
784 protein evolution. J. Mol. Biol. 353:911–923.

785 Bolger AM, Lohse M, Usadel B. 2014. Trimmomatic: a flexible trimmer for Illumina sequence data.

786 Bioinformatics 30:2114–2120.

787 Buljan M, Bateman A. 2009. The evolution of protein domain families. Biochem. Soc. Trans.
788 37:751–755.

789 Capra EJ, Laub MT. 2012. Evolution of two-component signal transduction systems. Annu. Rev.
790 Microbiol. 66:325–347.

791 Capra EJ, Perchuk BS, Lubin EA, Ashenberg O, Skerker JM, Laub MT. 2010. Systematic
792 dissection and trajectory-scanning mutagenesis of the molecular interface that ensures
793 specificity of two-component signaling pathways. PLoS Genet. 6:e1001220.

794 Capra EJ, Perchuk BS, Skerker JM, Laub MT. 2012. Adaptive mutations that prevent crosstalk
795 enable the expansion of paralogous signaling protein families. Cell 150:222–232.

796 Casas-Pastor D, Müller RR, Jaenicke S, Brinkrolf K, Becker A, Buttner MJ, Gross CA, Mascher
797 T, Goesmann A, Fritz G. 2021. Expansion and re-classification of the extracytoplasmic
798 function (ECF) σ factor family. Nucleic Acids Res. 49:986–1005.

799 Cases I, Ussery DW, De Lorenzo V. 2003. The σ^{54} regulon (sigmulon) of*Pseudomonas putida*.
800 Environ. Microbiol. 5:1281–1293.

801 Casino P, Rubio V, Marina A. 2009. Structural insight into partner specificity and phosphoryl
802 transfer in two-component signal transduction. Cell 139:325–336.

803 Chan CX, Beiko RG, Darling AE, Ragan MA. 2009. Lateral transfer of genes and gene fragments
804 in prokaryotes. Genome Biol. Evol. 1:429–438.

805 Chan CX, Darling AE, Beiko RG, Ragan MA. 2009. Are protein domains modules of lateral genetic
806 transfer? PLoS ONE 4:e4524.

807 Chen Y-T, Chang HY, Lu CL, Peng H-L. 2004. Evolutionary analysis of the two-component
808 systems in Pseudomonas aeruginosa PAO1. J. Mol. Evol. 59:725–737.

809 Chiniquy J, Garber ME, Mukhopadhyay A, Hillson NJ. 2020. Fluorescent amplification for next
810 generation sequencing (FA-NGS) library preparation. BMC Genomics 21:85.

811 Crooks GE, Hon G, Chandonia JM, Brenner SE. 2004. WebLogo: a sequence logo generator.
812 Genome Res. 14:1188–1190.

813 Delport W, Poon AFY, Frost SDW, Kosakovsky Pond SL. 2010. Datamonkey 2010: a suite of
814 phylogenetic analysis tools for evolutionary biology. Bioinformatics 26:2455–2457.

815 Efron B, Halloran E, Holmes S. 1996. Bootstrap confidence levels for phylogenetic trees. Proc
816 Natl Acad Sci USA 93:13429–13434.

817 El-Gebali S, Mistry J, Bateman A, Eddy SR, Luciani A, Potter SC, Qureshi M, Richardson LJ,
818 Salazar GA, Smart A, et al. 2019. The Pfam protein families database in 2019. Nucleic Acids
819 Res. 47:D427–D432.

820 Emms DM, Kelly S. 2019. OrthoFinder: phylogenetic orthology inference for comparative
821 genomics. Genome Biol. 20:238.

822 Engler C, Kandzia R, Marillonnet S. 2008. A one pot, one step, precision cloning method with
823 high throughput capability. PLoS ONE 3:e3647.

824 Finn RD, Attwood TK, Babbitt PC, Bateman A, Bork P, Bridge AJ, Chang H-Y, Dosztányi Z, El-
825 Gebali S, Fraser M, et al. 2017. InterPro in 2017-beyond protein family and domain
826 annotations. Nucleic Acids Res. 45:D190–D199.

827 Finn RD, Clements J, Eddy SR. 2011. HMMER web server: interactive sequence similarity
828 searching. Nucleic Acids Res. 39:W29-37.

829 Forslund K, Henricson A, Hollich V, Sonnhammer ELL. 2008. Domain tree-based analysis of
830 protein architecture evolution. Mol. Biol. Evol. 25:254–264.

831 Forslund SK, Kaduk M, Sonnhammer ELL. 2019. Evolution of protein domain architectures.

832 Methods Mol. Biol. 1910:469–504.

833 Gaebler C, Wang Z, Lorenzi JCC, Muecksch F, Finkin S, Tokuyama M, Cho A, Jankovic M,
834 Schaefer-Babajew D, Oliveira TY, et al. 2021. Evolution of antibody immunity to SARS-CoV-
835 2. Nature 591:639–644.

836 Galperin MY. 2005. A census of membrane-bound and intracellular signal transduction proteins
837 in bacteria: bacterial IQ, extroverts and introverts. BMC Microbiol. 5:35.

838 Galperin MY. 2006. Structural classification of bacterial response regulators: diversity of output
839 domains and domain combinations. J. Bacteriol. 188:4169–4182.

840 Galperin MY. 2010. Diversity of structure and function of response regulator output domains. Curr.
841 Opin. Microbiol. 13:150–159.

842 Galperin MY. 2018. What bacteria want. Environ. Microbiol. 20:4221–4229.

843 Gibson DG, Young L, Chuang R-Y, Venter JC, Hutchison CA, Smith HO. 2009. Enzymatic
844 assembly of DNA molecules up to several hundred kilobases. Nat. Methods 6:343–345.

845 Groban ES, Clarke EJ, Salis HM, Miller SM, Voigt CA. 2009. Kinetic buffering of cross talk
846 between bacterial two-component sensors. J. Mol. Biol. 390:380–393.

847 Gumerov VM, Ortega DR, Adebali O, Ulrich LE, Zhulin IB. 2020. MiST 3.0: an updated microbial
848 signal transduction database with an emphasis on chemosensory systems. Nucleic Acids
849 Res. 48:D459–D464.

850 Haushalter RW, Groff D, Deutsch S, The L, Chavkin TA, Brunner SF, Katz L, Keasling JD. 2015.
851 Development of an orthogonal fatty acid biosynthesis system in E. coli for oleochemical
852 production. Metab. Eng. 30:1–6.

853 Heger A, Holm L. 2003. Exhaustive enumeration of protein domain families. J. Mol. Biol. 328:749–
854 767.

855 Henderson PJF, Maher C, Elbourne LDH, Eijkelkamp BA, Paulsen IT, Hassan KA. 2021.
856 Physiological functions of bacterial “multidrug” efflux pumps. Chem. Rev. 121:5417–5478.

857 Hillson NJ, Rosengarten RD, Keasling JD. 2012. j5 DNA assembly design automation software.
858 ACS Synth. Biol. 1:14–21.

859 Hirakawa H, Kurushima J, Hashimoto Y, Tomita H. 2020. Progress Overview of Bacterial Two-
860 Component Regulatory Systems as Potential Targets for Antimicrobial Chemotherapy.
861 Antibiotics (Basel) 9.

862 Hug LA, Baker BJ, Anantharaman K, Brown CT, Probst AJ, Castelle CJ, Butterfield CN, Hernsdorf
863 AW, Amano Y, Ise K, et al. 2016. A new view of the tree of life. Nat. Microbiol. 1:16048.

864 Incha MR, Thompson MG, Blake-Hedges JM, Liu Y, Pearson AN, Schmidt M, Gin JW, Petzold
865 CJ, Deutschbauer AM, Keasling JD. 2020. Leveraging host metabolism for
866 bisdemethoxycurcumin production in Pseudomonas putida. Metab. Eng. Commun.
867 10:e00119.

868 Jing X, Dong Q, Hong D, Lu R. 2020. Amino acid encoding methods for protein sequences: A
869 comprehensive review and assessment. IEEE/ACM Trans Comput Biol Bioinform 17:1918–
870 1931.

871 Jumper J, Evans R, Pritzel A, Green T, Figurnov M, Ronneberger O, Tunyasuvunakool K, Bates
872 R, Žídek A, Potapenko A, et al. 2021. Highly accurate protein structure prediction with
873 AlphaFold. Nature 596:583–589.

874 Jurėnas D, Fraikin N, Goormaghtigh F, Van Melderen L. 2022. Biology and evolution of bacterial
875 toxin-antitoxin systems. Nat. Rev. Microbiol. 20:335–350.

876 Katoh K, Standley DM. 2013. MAFFT multiple sequence alignment software version 7:
877 improvements in performance and usability. Mol. Biol. Evol. 30:772–780.

878 Kharchenko PV, Tolstorukov MY, Park PJ. 2008. Design and analysis of ChIP-seq experiments

879 for DNA-binding proteins. Nat. Biotechnol. 26:1351–1359.

880 Kosakovsky Pond SL, Murrell B, Fourment M, Frost SDW, Delport W, Scheffler K. 2011. A random
881 effects branch-site model for detecting episodic diversifying selection. Mol. Biol. Evol.
882 28:3033–3043.

883 Langmead B, Trapnell C, Pop M, Salzberg SL. 2009. Ultrafast and memory-efficient alignment of
884 short DNA sequences to the human genome. Genome Biol. 10:R25.

885 Laub MT, Goulian M. 2007. Specificity in two-component signal transduction pathways. Annu.
886 Rev. Genet. 41:121–145.

887 Li H, Handsaker B, Wysoker A, Fennell T, Ruan J, Homer N, Marth G, Abecasis G, Durbin R,
888 1000 Genome Project Data Processing Subgroup. 2009. The Sequence Alignment/Map
889 format and SAMtools. Bioinformatics 25:2078–2079.

890 Loeschcke A, Thies S. 2015. Pseudomonas putida-a versatile host for the production of natural
891 products. Appl. Microbiol. Biotechnol. 99:6197–6214.

892 van der Maaten L, Hinton G. 2008. Visualizing data using t-SNE. J Mach Learn Res 8:2579−2605.

893 McClune CJ, Alvarez-Buylla A, Voigt CA, Laub MT. 2019. Engineering orthogonal signalling
894 pathways reveals the sparse occupancy of sequence space. Nature.

895 McClune CJ, Laub MT. 2020. Constraints on the expansion of paralogous protein families. Curr.
896 Biol. 30:R460–R464.

897 Mironov AA, Vinokurova NP, Gelfand MS. 2000. Software for analysis of bacterial genomes. Mol
898 Biol (NY) 34:222–231.

899 Mistry J, Finn RD, Eddy SR, Bateman A, Punta M. 2013. Challenges in homology search:
900 HMMER3 and convergent evolution of coiled-coil regions. Nucleic Acids Res. 41:e121.

901 Murrell B, Wertheim JO, Moola S, Weighill T, Scheffler K, Kosakovsky Pond SL. 2012. Detecting

902 individual sites subject to episodic diversifying selection. PLoS Genet. 8:e1002764.

903 Nguyen L-T, Schmidt HA, von Haeseler A, Minh BQ. 2015. IQ-TREE: a fast and effective
904 stochastic algorithm for estimating maximum-likelihood phylogenies. Mol. Biol. Evol. 32:268–
905 274.

906 Noriega CE, Lin H-Y, Chen L-L, Williams SB, Stewart V. 2010. Asymmetric cross-regulation
907 between the nitrate-responsive NarX-NarL and NarQ-NarP two-component regulatory
908 systems from Escherichia coli K-12. Mol. Microbiol. 75:394–412.

909 Ohta T. 1991. Role of diversifying selection and gene conversion in evolution of major
910 histocompatibility complex loci. Proc Natl Acad Sci USA 88:6716–6720.

911 Ohta T. 2001. Molecular evolution: nearly neutral theory. In: John Wiley & Sons, Ltd, editor. eLS.
912 Chichester, UK: John Wiley & Sons, Ltd.

913 Pao GM, Saier MH. 1995. Response regulators of bacterial signal transduction systems: selective
914 domain shuffling during evolution. J. Mol. Evol. 40:136–154.

915 Papon N, Stock AM. 2019. Two-component systems. Curr. Biol. 29:R724–R725.

916 Pettersen EF, Goddard TD, Huang CC, Meng EC, Couch GS, Croll TI, Morris JH, Ferrin TE. 2021.
917 UCSF ChimeraX: structure visualization for researchers, educators, and developers. Protein
918 Sci. 30:70–82.

919 Pond SLK, Frost SDW. 2005. Datamonkey: rapid detection of selective pressure on individual
920 sites of codon alignments. Bioinformatics 21:2531–2533.

921 Potvin E, Sanschagrin F, Levesque RC. 2008. Sigma factors in Pseudomonas aeruginosa. FEMS
922 Microbiol. Rev. 32:38–55.

923 Qian W, Han Z-J, He C. 2008. Two-component signal transduction systems of Xanthomonas spp.:
924 a lesson from genomics. Mol. Plant Microbe Interact. 21:151–161.

925 Rand JM, Pisithkul T, Clark RL, Thiede JM, Mehrer CR, Agnew DE, Campbell CE, Markley AL,
926 Price MN, Ray J, et al. 2017. A metabolic pathway for catabolizing levulinic acid in bacteria.
927 Nat. Microbiol. 2:1624–1634.

928 Ronneau S, Hallez R. 2019. Make and break the alarmone: regulation of (p)ppGpp
929 synthetase/hydrolase enzymes in bacteria. FEMS Microbiol. Rev. 43:389–400.

930 Schmidl SR, Ekness F, Sofjan K, Daeffler KN-M, Brink KR, Landry BP, Gerhardt KP, Dyulgyarov
931 N, Sheth RU, Tabor JJ. 2019. Rewiring bacterial two-component systems by modular DNA-
932 binding domain swapping. Nat. Chem. Biol. 15:690–698.

933 Sharma P, Bano A, Singh SP, Sharma S, Xia C, Nadda AK, Lam SS, Tong YW. 2022. Engineered
934 microbes as effective tools for the remediation of polyaromatic aromatic hydrocarbons and
935 heavy metals. Chemosphere 306:135538.

936 Silva GGZ, Cuevas DA, Dutilh BE, Edwards RA. 2014. FOCUS: an alignment-free model to
937 identify organisms in metagenomes using non-negative least squares. PeerJ 2:e425.

938 Simon C. 2022. An evolving view of phylogenetic support. Syst. Biol. 71:921–928.

939 Siryaporn A, Goulian M. 2008. Cross-talk suppression between the CpxA-CpxR and EnvZ-OmpR
940 two-component systems in E. coli. Mol. Microbiol. 70:494–506.

941 Siryaporn A, Perchuk BS, Laub MT, Goulian M. 2010. Evolving a robust signal transduction
942 pathway from weak cross-talk. Mol. Syst. Biol. 6:452.

943 Smith MD, Wertheim JO, Weaver S, Murrell B, Scheffler K, Kosakovsky Pond SL. 2015. Less is
944 more: an adaptive branch-site random effects model for efficient detection of episodic
945 diversifying selection. Mol. Biol. Evol. 32:1342–1353.

946 Stephenson K, Hoch JA. 2002. Evolution of signalling in the sporulation phosphorelay. Mol.
947 Microbiol. 46:297–304.

948 Stock AM, Robinson VL, Goudreau PN. 2000. Two-component signal transduction. Annu. Rev.
949 Biochem. 69:183–215.

950 Studier FW. 2005. Protein production by auto-induction in high density shaking cultures. Protein
951 Expr. Purif. 41:207–234.

952 Thompson MG, Blake-Hedges JM, Cruz-Morales P, Barajas JF, Curran SC, Eiben CB, Harris NC,
953 Benites VT, Gin JW, Sharpless WA, et al. 2019. Massively parallel fitness profiling reveals
954 multiple novel enzymes in Pseudomonas putida lysine metabolism. MBio 10.

955 Thompson MG, Incha MR, Pearson AN, Schmidt M, Sharpless WA, Eiben CB, Cruz-Morales P,
956 Blake-Hedges JM, Liu Y, Adams CA, et al. 2020. Fatty acid and alcohol metabolism in
957 Pseudomonas putida: functional analysis using random barcode transposon sequencing.
958 Appl. Environ. Microbiol. 86.

959 Tiwari S, Jamal SB, Hassan SS, Carvalho PVSD, Almeida S, Barh D, Ghosh P, Silva A, Castro
960 TLP, Azevedo V. 2017. Two-Component Signal Transduction Systems of Pathogenic
961 Bacteria As Targets for Antimicrobial Therapy: An Overview. Front. Microbiol. 8:1878.

962 Vandewege MW, Mangum SF, Gabaldón T, Castoe TA, Ray DA, Hoffmann FG. 2016. Contrasting
963 patterns of evolutionary diversification in the olfactory repertoires of reptile and bird genomes.
964 Genome Biol. Evol. 8:470–480.

965 Varadi M, Anyango S, Deshpande M, Nair S, Natassia C, Yordanova G, Yuan D, Stroe O, Wood
966 G, Laydon A, et al. 2022. AlphaFold Protein Structure Database: massively expanding the
967 structural coverage of protein-sequence space with high-accuracy models. Nucleic Acids
968 Res. 50:D439–D444.

969 Varughese KI, Madhusudan, Zhou XZ, Whiteley JM, Hoch JA. 1998. Formation of a novel four-
970 helix bundle and molecular recognition sites by dimerization of a response regulator
971 phosphotransferase. Mol. Cell 2:485–493.

972 Volke DC, Turlin J, Mol V, Nikel PI. 2020. Physical decoupling of XylS/Pm regulatory elements
973 and conditional proteolysis enable precise control of gene expression in Pseudomonas
974 putida. Microb. Biotechnol. 13:222–232.

975 Wang BX, Cady KC, Oyarce GC, Ribbeck K, Laub MT. 2021. Two-Component Signaling Systems
976 Regulate Diverse Virulence-Associated Traits in Pseudomonas aeruginosa. Appl. Environ.
977 Microbiol. 87.

978 Weaver S, Shank SD, Spielman SJ, Li M, Muse SV, Kosakovsky Pond SL. 2018. Datamonkey
979 2.0: A modern web application for characterizing selective and other evolutionary processes.
980 Mol. Biol. Evol. 35:773–777.

981 Wetmore KM, Price MN, Waters RJ, Lamson JS, He J, Hoover CA, Blow MJ, Bristow J, Butland
982 G, Arkin AP, et al. 2015. Rapid quantification of mutant fitness in diverse bacteria by
983 sequencing randomly bar-coded transposons. MBio 6:e00306-15.

984 Zhang Z, Wood WI. 2003. A profile hidden Markov model for signal peptides generated by
985 HMMER. Bioinformatics 19:307–308.

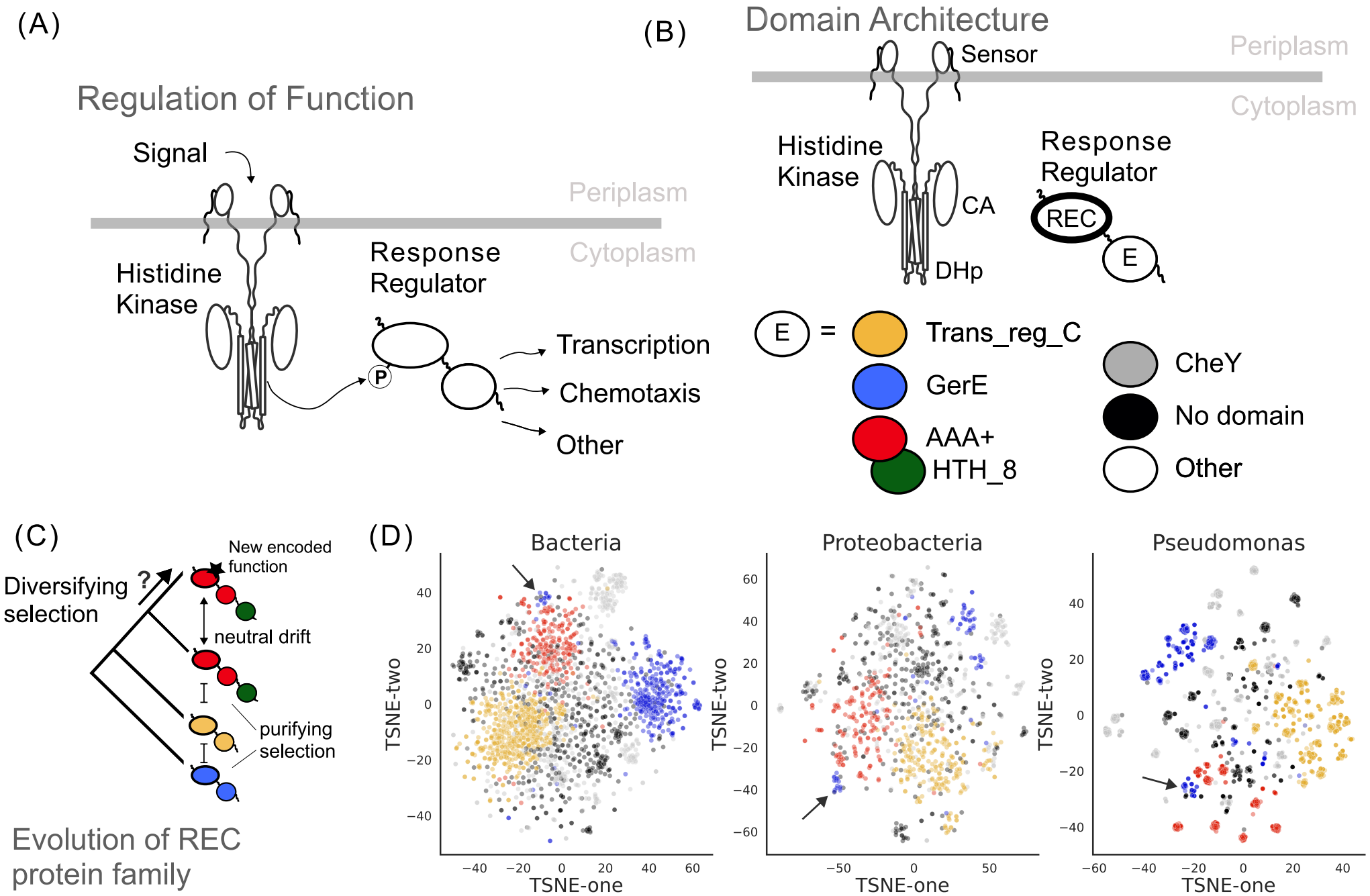
(A)
Regulation of Function
Signal
Periplasm
Cytoplasm
Histidine Kinase
Response Regulator
P
Transcription
Chemotaxis
Other
(B)
Domain Architecture
Sensor
Periplasm
Cytoplasm
Histidine Kinase
CA
DHp
Response Regulator
REC
E
E =
Trans_reg_C
GerE
AAA+ HTH_8
CheY
No domain
Other
(C)
New encoded function
Diversifying selection
?
neutral drift
purifying selection
Evolution of REC protein family
(D)
Bacteria
Proteobacteria
Pseudomonas
TSNE-two
TSNE-one

Figure 1

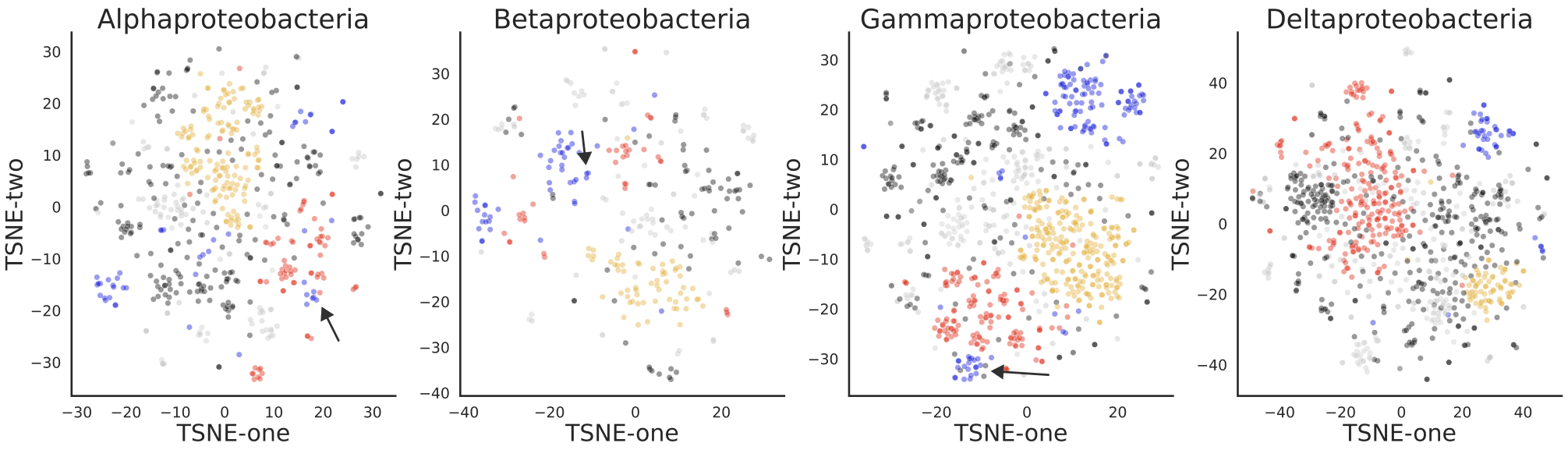
Alphaproteobacteria
Betaproteobacteria
Gammaproteobacteria
Deltaproteobacteria
TSNE-two
TSNE-one

Figure 2

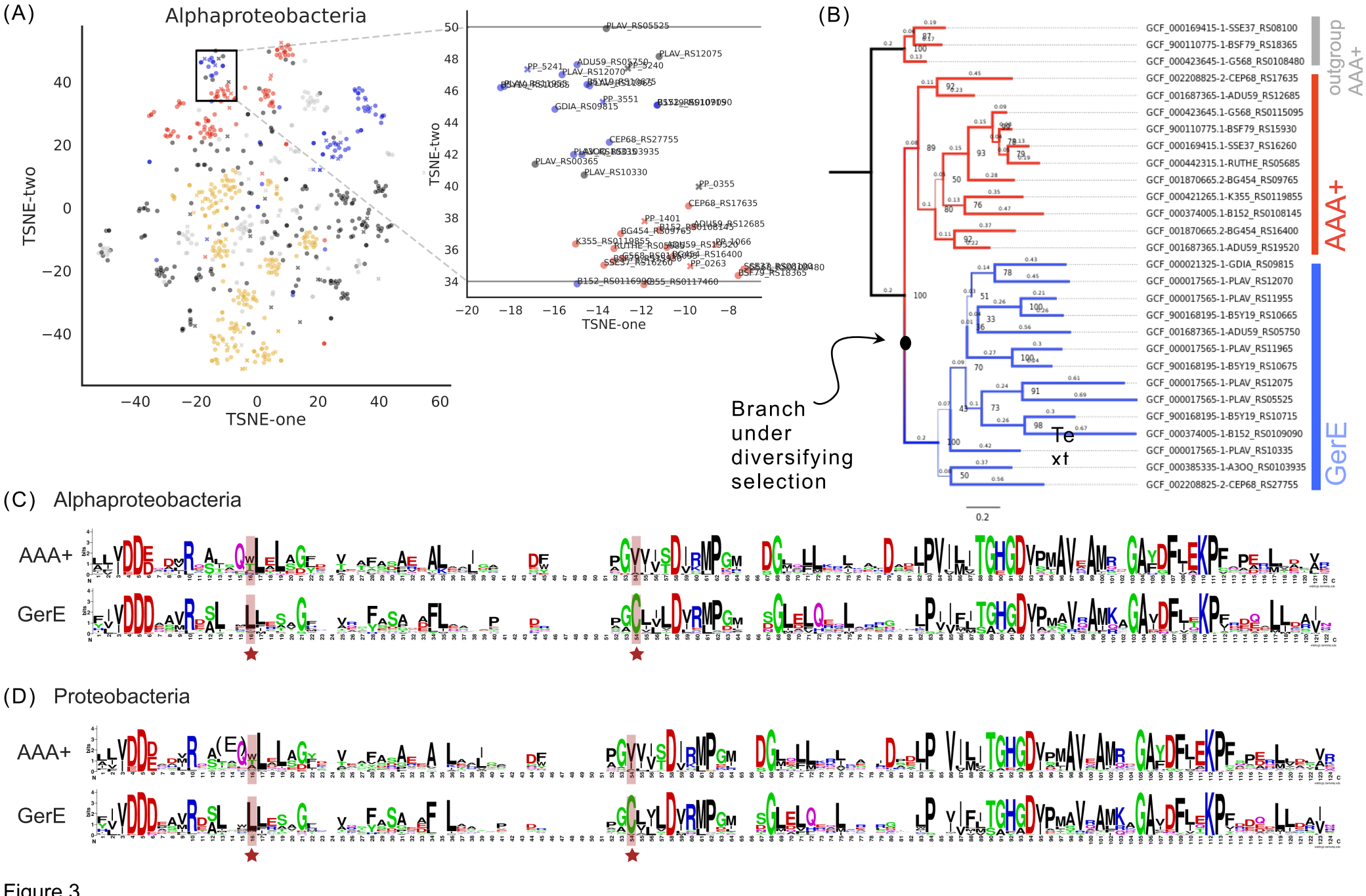
(A)
Alphaproteobacteria
TSNE-two
TSNE-one
(B)
outgroup
AAA+
AAA+
GerE
Branch under diversifying selection
0.2
(C) Alphaproteobacteria
AAA+
GerE
(D) Proteobacteria
AAA+
GerE

Figure 3

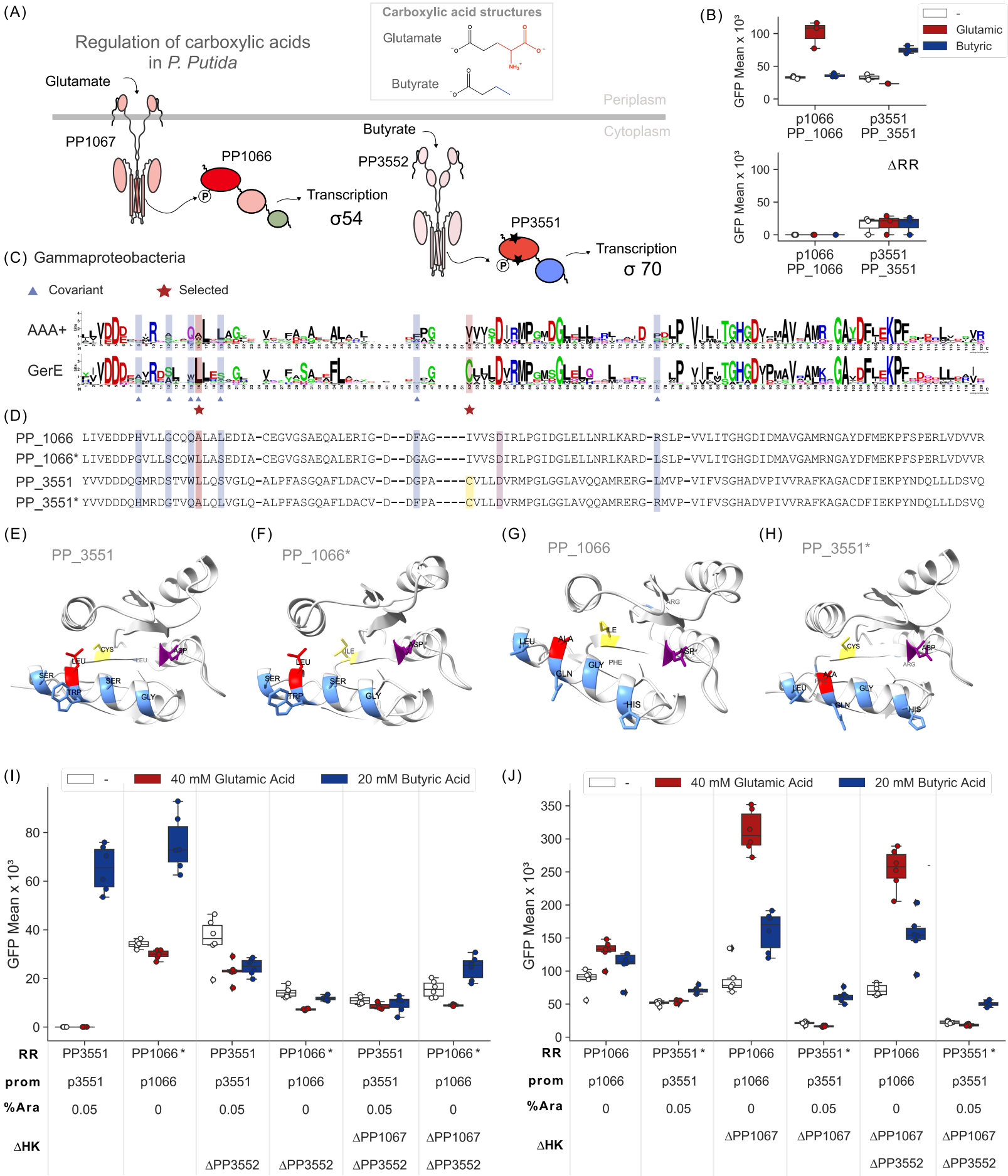
(A)
Regulation of carboxylic acids in P. Putida
Carboxylic acid structures
Glutamate
Butyrate
Periplasm
Cytoplasm
Glutamate
PP1067
PP1066
Transcription
σ54
Butyrate
PP3552
PP3551
Transcription
σ 70
(B)
GFP Mean x 10³
p1066 PP_1066
p3551 PP_3551
ΔRR
-
Glutamic
Butyric
(C) Gammaproteobacteria
Covariant
Selected
AAA+
GerE
(D)
PP_1066 LIVEDDPHVLLGCQQALALEDIA-CEGVGSAEQALERIG-D--DFAG----IVVSDIRLPGIDGLELLNRLKARD-RSLP-VVLITGHGDIDMAVGAMRNGAYDFMEKPFSPERLVDVVR
PP_1066* LIVEDDPGVLLSCQWLLASEDIA-CEGVGSAEQALERIG-D--DGAG----IVVSDIRLPGIDGLELLNRLKARD-LSLP-VVLITGHGDIDMAVGAMRNGAYDFMEKPFSPERLVDVVR
PP_3551 YVVDDDQGMRDSTVWLLQSVGLQ-ALPFASGQAFLDACV-D--DGPA----CVLLDVRMPGLGGLAVQQAMRERG-LMVP-VIFVSGHADVPIVVRAFKAGACDFIEKPYNDQLLLDSVQ
PP_3551* YVVDDDQHMRDGTVQALQLVGLQ-ALPFASGQAFLDACV-D--DFPA----CVLLDVRMPGLGGLAVQQAMRERG-RMVP-VIFVSGHADVPIVVRAFKAGACDFIEKPYNDQLLLDSVQ
(E) PP_3551
(F) PP_1066*
(G) PP_1066
(H) PP_3551*
(I)
- 40 mM Glutamic Acid 20 mM Butyric Acid
GFP Mean x 10³
RR PP3551 PP1066 * PP3551 PP1066 * PP3551 PP1066 *
prom p3551 p1066 p3551 p1066 p3551 p1066
%Ara 0.05 0 0.05 0 0.05 0
ΔHK ΔPP3552 ΔPP3552 ΔPP1067 ΔPP3552 ΔPP1067 ΔPP3552
(J)
- 40 mM Glutamic Acid 20 mM Butyric Acid
GFP Mean x 10³
RR PP1066 PP3551 * PP1066 PP3551 * PP1066 PP3551 *
prom p1066 p3551 p1066 p3551 p1066 p3551
%Ara 0 0.05 0 0.05 0 0.05
ΔHK ΔPP1067 ΔPP1067 ΔPP1067 ΔPP1067 ΔPP3552 ΔPP3552

Figure 4

(A)

1 σ70 regulated REC expand in early bacteria

2 σ54 regulated REC expand in early proteobacteria

3 σ54 regulated carboxylic acid responsive REC emerge in early proteobacteria

4 Within gene recombination of a duplicated carboxylic acid responsive σ54 regulated REC alters its regulatory context in early alphaproteobacteria

5 Episodic diversifying selection driven by functional discordance

6 Emergence of new signaling system

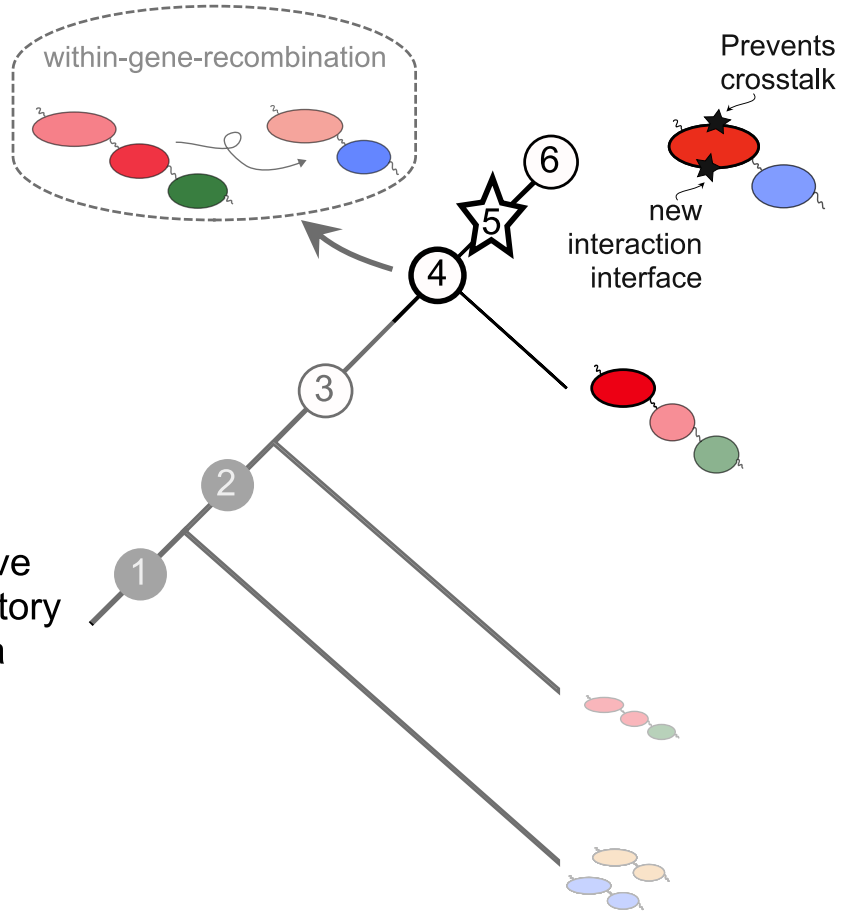

(B)

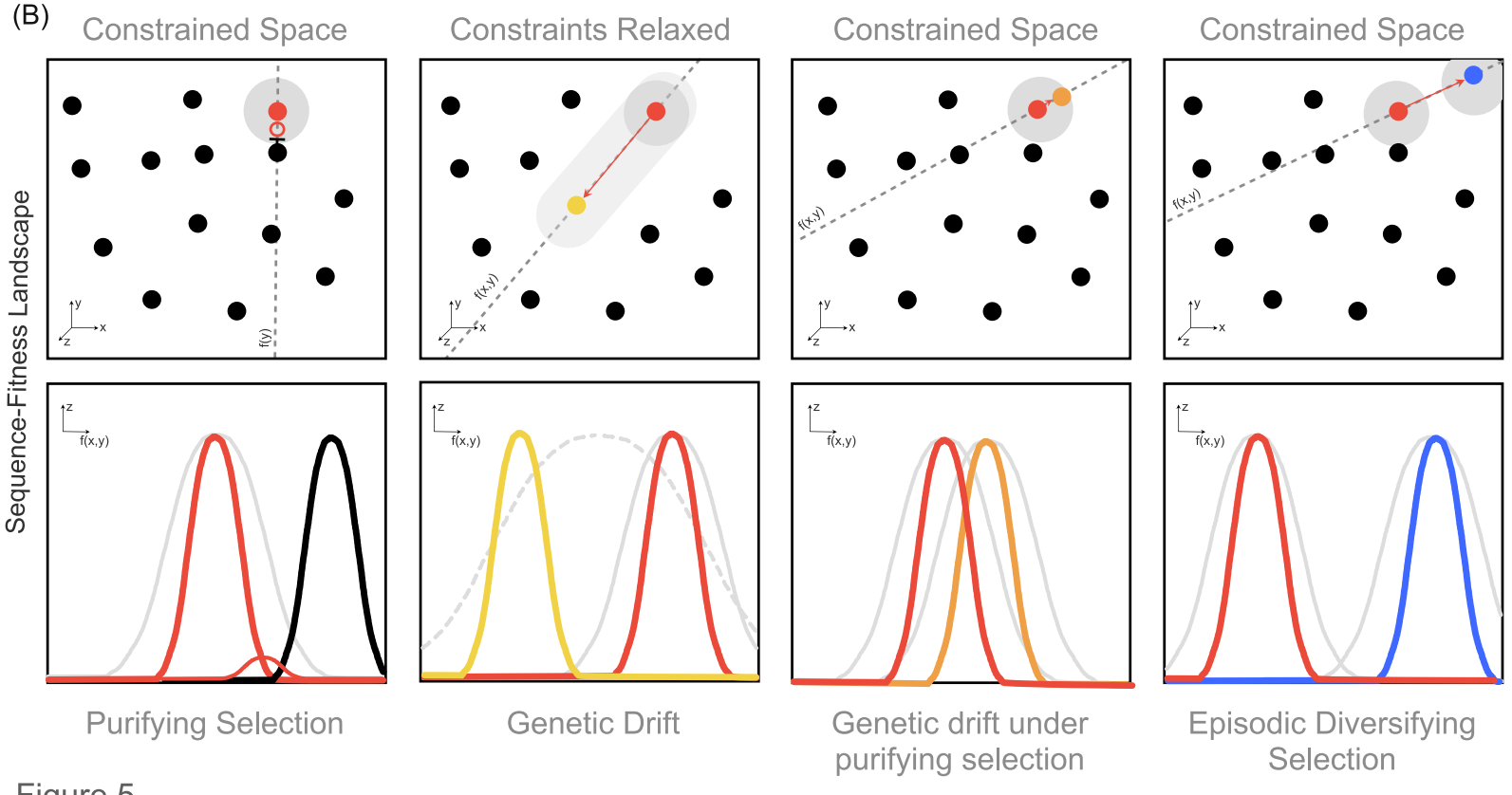

Figure 5